IEICE TRANS. ELECTRON., VOL.E92–C, NO.9 SEPTEMBER 2009

INVITED PAPER *Special Section on Recent Progress in Microwave and Millimeter-Wave Technologies and Their Applications*

Advanced MMIC Receiver for 94-GHz Band Passive Millimeter-Wave Imager

Masaru SATO[†a)], ***Member***, **Tatsuya HIROSE**[†], ***Nonmember***, ***and*** **Koji MIZUNO**[††], ***Fellow***

SUMMARY In this paper, we present the development of an advanced MMIC receiver for a 94-GHz band passive millimeter-wave (PMMW) imager. Our configuration is based on a Dicke receiver in order to reduce fluctuations in the detected voltage. By introducing an electronic switch in the MMIC, we achieved a high resolution millimeter-wave image in a shorter image collection time compared to that with a conventional mechanical chopper. We also developed an imaging array using MMIC receivers.

key words: *Dicke-radiometer, low noise amplifier, MMIC, passive millimeter-wave imager, SPDT switch*

1. Introduction

All objects radiate electromagnetic waves from microwave to infrared regions. The amplitude of the radiation depends on the object's emissivity and temperature. Passive millimeter-wave (PMMW) imagers detect the relative intensity of millimeter-wave radiation and visualize it. As PMMW imagers are able to detect objects which are not detectable using visible light or infrared cameras, PMMW imagers are now being used in fields such as security, remote sensing, and disaster prevention [1], [2]. The 94-GHz band is especially well suited for millimeter-wave imaging, because atmospheric absorption around this frequency is relatively low, and a high spatial resolution is possible due to it's short wavelength. PMMW imaging systems using this band have already been developed [2]–[5] for concealed weapons detection (CWD) and for flight systems. So far, we have developed prototype PMMW imagers by developing ultra low-noise and high-gain MMICs [6] and a compact planar antenna [7]. And we have acquired 94-GHz band millimeter-wave images.

For this system, we employed a Dicke receiver [8] in order to decrease fluctuations in the detected voltage. These fluctuations are derived from temperature, gain variation in the LNA, or DC drift (1/f noise) in the detector. Dicke receiver consists of an RF switch, a low noise amplifier (LNA), a detector, and a lock-in-amplifier. The RF switch alternately switches between the millimeter-wave signal from the scene and reference noise. By subtracting these in a lock-in-amplifier, fluctuations in the detected voltage can be decreased.

For the RF switch, we used a mechanical chopper with electric-wave absorbers attached. The input millimeter-waves were switched by rotating the chopper. Although the mechanical chopper is simple and has low loss, it is large in size. If we need a large array of receivers in order to reduce the image collection time, a larger chopper is needed, and this becomes unrealistic. In addition, the rotary speed of the chopper varies slightly due to eccentricity or imbalances in the weight of the chopper. This causes loss of synchronization and variation in the voltage detected in the lock-in-amplifier. For this reason, a long integration time is needed for a mechanical chopper. In addition, the upper limit of the switching speed is below around 200 Hz. These defects are impractical for real-time imaging.

To solve these problems, we developed an electronic switch. Although a switch using PIN diodes is commercially available, it requires additional space and cost. Thus we developed a single-pole-double-throw (SPDT) switch that could be integrated on an MMIC consisting of an LNA and a detector. We used the distributed type SPDT switch to give low insertion loss and high isolation as well as a high switching speed. Here, we discuss the design techniques to achieve a high switching speed. Using the design techniques, our developed SPDT switch has an insertion loss of 2 dB, isolation of better than 40 dB, and a switching speed of more than 500 kHz. We also developed a high-gain low-noise amplifier using 0.1-μm gate InP HEMT technology. The measured gain and noise figure were 35 dB and 3 dB, respectively. Furthermore, we combined the switch, LNA and detector and integrated them into the MMIC receiver. We then used this MMIC receiver to develop a prototype PMMW imager. The detected voltage from the new imager has a much lower variation than the conventional imager which uses a mechanical chopper.

2. MMIC Receiver

Figure 1 shows the block diagram of our MMIC receiver. It consists of a SPDT switch, LNA, and detector. The input of the LNA is switched between the antenna and the reference load with a repetition frequency of f_M. In a half period, the LNA receives an input signal from the RX antenna. In the other half period, the LNA receives reference noise. Since the fluctuations in the detected voltage vary slowly compared with f_M, the fluctuations can be removed by using a lock-in-amplifier.

Manuscript received December 25, 2008.

[†]The authors are with Fujitsu Ltd., Atsugi-shi, 243-0197 Japan.
[††]The author is with Tohoku University, Sendai-shi, 980-8577 Japan.
a) E-mail: sato.masaru@jp@fujitsu.com

DOI: 10.1587/transele.E92.C.1124

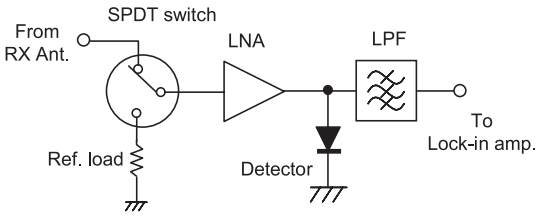

Fig. 1 Block diagram of the MMIC receiver.

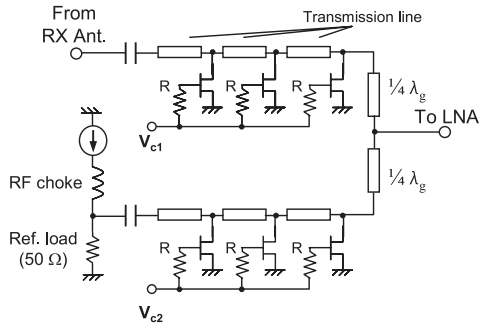

Fig. 2 SPDT switch schematic for the Dicke receiver.

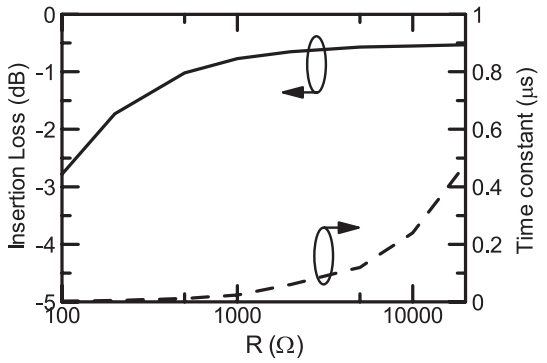

Fig. 3 Insertion loss at the frequency of 94 GHz and time constant of the SPST switch as a function of the series resistance, R.

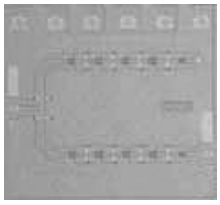

Fig. 4 Die photo of SPDT switch. The chip size is $0.8 \times 0.8\,\mathrm{mm}^2$.

2.1 SPDT Switch

Figure 2 shows a schematic diagram of the distributed SPDT switch [9]–[11], which is composed of two single-pole-single-throw (SPST) switches and two quarter-wavelength impedance transformers. The drain terminals of the transistors were connected to the transmission lines periodically. One port of the SPST switch was terminated in 50 Ω as a reference load. In addition, we added an RF choke and a current source to adjust the noise power from the reference load to be equal to the antenna noise.

The gates of the transistors in each SPST switch were biased below the pinch-off voltage; for example −1 V, or alternately, in the linear region such as at 0.5 V. When the bias applied is below the pinch-off voltage, the transistors act as capacitors. We chose the length and width of the transmission lines to give a characteristic impedance Z_0 for the artificial transmission line of 50 Ω (ON-state). On the other hands, when the bias applied is a positive voltage such as 0.5 V, the transistors act as small resistances. Since the transistors are shunted between the transmission lines, the SPST circuit works as a short circuit (OFF-state).

Series resistances, R, connected to the gate terminals, affects the insertion loss of the ON-state SPST switch, because the drain-gate capacitance value C_{dg} is almost the same as the drain-source capacitance value C_{ds}. Small R degrade the insertion loss in the ON-state SPST switch. The propagation constant γ is expressed as follows:

$$\gamma \equiv \alpha + j\beta = \sqrt{j\omega L_{TL}\left(\frac{1}{R//j\omega C_{gd}} + j\omega\left(C_{ds} + C_{TL}\right)\right)} \qquad (1)$$

where, L_{TL} and C_{TL} are the transmission line inductance and capacitance, respectively. In order to achieve a low loss in the ON-state SPDT switch, a large resistance R is needed.

However, a large series resistance degrades the switching speed between the ON and OFF states, because the series resistance and input capacitance of the transistor form an RC time-constant. Moreover, PMMW imagers have to measure the equivalent millimeter-wave power in a short integration time.

The solid line in Fig. 3 shows the calculated insertion loss in the SPST switch in the ON-state at a frequency of 94 GHz as a function of R. The dashed line in Fig. 3 represents the RC-time constant. For this, we used $0.15 \times 40\,\mu$m HEMTs whose C_{gd} and C_{ds} were both 13 fF. The length of each transmission lines was 130 μm. From the figure, we chose the value of R as 5 kΩ, because it shows a small-time constant and small insertion loss.

We designed and fabricated an SPDT switch using the InP HEMT process. Figure 4 shows the microphotograph of the SPDT switch. Figure 5 shows the insertion loss and isolation of the developed SPDT switch. The gate bias condition was −1 V for the ON-branch, and 0.5 V for the OFF-branch. The measured insertion loss was within −2 dB between 60 and 110 GHz and isolation was better than −40 dB.

We also show the modulated waveform generated by switching with V_{c1} and $V4_{c2}$. The input signal was a 60-GHz continuous wave (CW) source whose power level was −20 dBm. 500-kHz square pulses were applied to the gate terminals, V_{c1} and V_{c2}. Figure 6 shows the detected waveform and the control waveform for the switch. The modulated waveform indicates that our switch can modulate the RF signal at more than 500 kHz. Therefore, we connected the SPDT switch to the front end of the receiver.

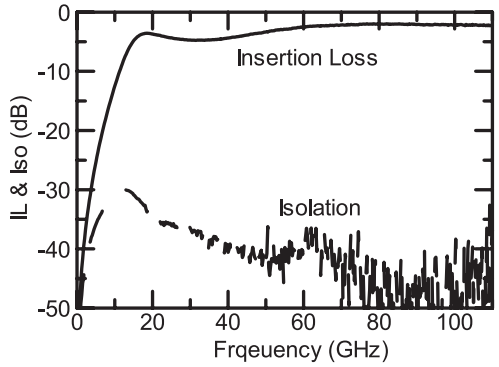

Fig. 5 Frequency dependence of insertion loss (IL) and isolation (Iso) of the developed SPDT switch from 1to 110 GHz.

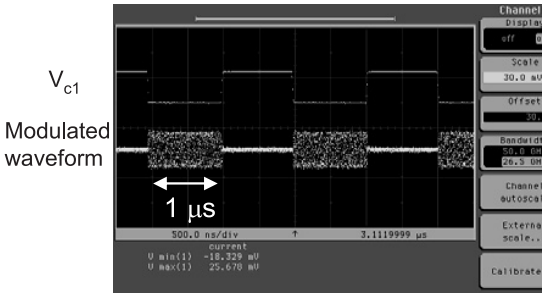

Fig. 6 Detected modulated waveform. Input RF frequency was 60 GHz. Switching frequency was 500 kHz.

2.2 Low Noise Amplifier

Next we will describe the performance of the LNA. The LNA has the role of amplifying the input millimeter-wave signal to a sufficient level to be detected by the following detector without deteriorating the signal-to-noise ratio, and for this, both low-noise and high-gain performance are needed. The LNA we developed with a gain of 33 dB and a noise figure of 3.2 dB is described in [6]. The LNA which we designed and fabricated for this project used a high-speed and low-noise InP HEMT [12]. Figure 7 shows a die photo of the 94-GHz band LNA. The LNA consists of three-stage cascode amplifiers. For each amplifier stage, we used 0.1 $\times$ 40 μm HEMTs with a cutoff frequency of 280 GHz and a minimum noise figure of 1 dB at 94 GHz.

We applied a drain voltage of V_d = 1.6 V, a gate voltage of V_{g1} = 0 V, and a second gate voltage of V_{g2} = 0.8 V. Thin film microstrip line (TFMSL) technology was applied to suppress the excitation of parasitic substrate modes. The overall chip size of the 94-GHz band LNA is 2.5 $\times$ 1.2 mm^2.

The measured small-signal gain and noise figure are shown in Fig. 8. Our LNA achieved a linear gain of more than 30 dB between 75 and 110 GHz. The gain at a frequency of 85 GHz was 40 dB, and the average noise figure was 3.0 dB.

Figure 9 shows a comparison with the published W-band LNAs. We plotted the noise figure as a function of the gain for the published results [13]–[19] and for our own LNA. The area with high-gain and low-noise on the lower right in Fig. 9 is suitable for imagers. The graph shows that our LNA is a state-of-the-art high-gain and low-noise amplifier. We then used the LNA to develop an MMIC receiver.

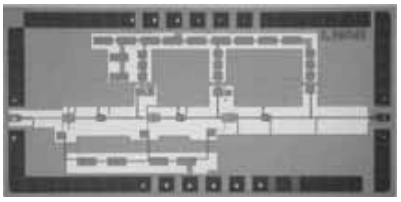

Fig. 7 Die photo of 94-GHz band LNA. The chip size is 2.5 $\times$ 1.2 mm^2.

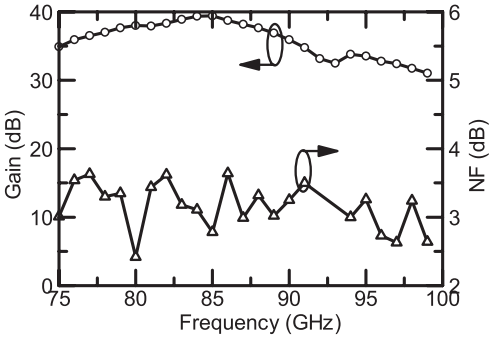

Fig. 8 Measured gain and noise figure of developed LNA.

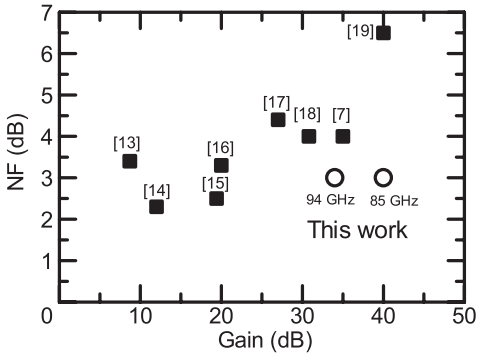

Fig. 9 Comparison with published W-band LNAs.

2.3 MMIC Receiver

We integrated the switch, LNA, and detector onto a single chip. The switch and LNA have been described in the previous sections. The detector was made of a zero-biased Schottky diode constructed on a HEMT device. The gate length and width were 4 μm and 5 μm, respectively. Figure 10 shows a die photo of the fabricated MMIC receiver. The chip size is the same as for the LNA (2.5 $\times$ 1.2 mm^2). Inverted microstrip line (IMSL) technology was used for the SPDT switch to isolate it from the LNA. The total power consumption was 64 mW.

We will now describe the measured performance of the MMIC receiver. We measured the sensitivity of the MMIC

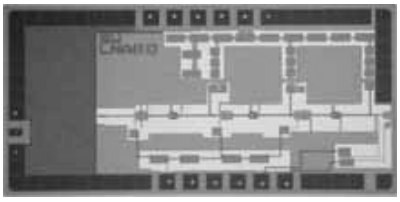

Fig. 10 Die photo of the MMIC receiver. The chip size is $2.5 \times 1.2\,\mathrm{mm}^2$.

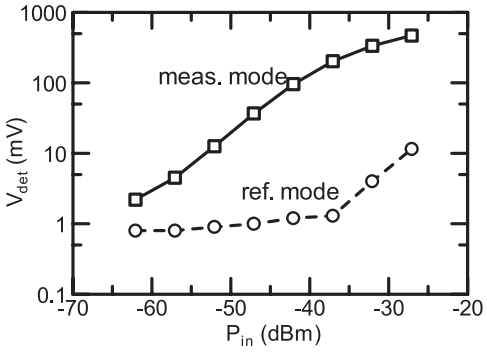

Fig. 11 Measured detected output voltage as a function of input power.

receiver by calculating the ratio of the detected output voltage for input millimeter-wave power. For this measurement, we used a 94-GHz CW source as the input. The bias voltages for the SPDT switch, V_{c1} and V_{c2} are -1 and 0.5 V, respectively while the MMIC receiver was measuring the millimeter-wave signal (measuring mode). When the receiver was measuring the reference load (reference mode), V_{c1} and V_{c2} were set to 0.5 and -1 V, respectively. Figure 11 shows the detected voltage as a function of the input RF power level. Since the isolation of the SPDT switch was below -40 dB, the difference in the detected voltage between the measuring and reference modes was detectable. The calculated sensitivity of the MMIC receiver was 2,440 kV/W.

3. PMMW Imaging

We fabricated a PMMW imaging test system using our MMIC receiver. Figure 12(a) shows the block diagram of the PMMW imaging system using the MMIC receiver with the SPDT switch. It consists of a 20-cm diameter lens, an antipodal linearly tapered slot antenna [7] formed on a polyimide substrate, MMIC receiver, DC amplifier, and a lock-in amplifier. The antenna, receiver and DC amplifier were set on an elevated stage and scanned on the focal plane of the lens. The MMIC was mounted on the antenna using a flip chip bonding (FCB) assembly. A switch driver controls polarity of the switch in the MMIC and lock-in amplifier simultaneously. Figure 12(b) represents a conventional imaging system that uses a mechanical chopper for comparison.

We measured the time dependence of the detected voltage V_d from the lock-in amplifier using electronic and mechanical switches as shown in Figs. 13(a) and (b). The detected voltage fluctuations using the mechanical chopper shown in Fig. 13(b) are as large as 5 V_{pp}, which degrades

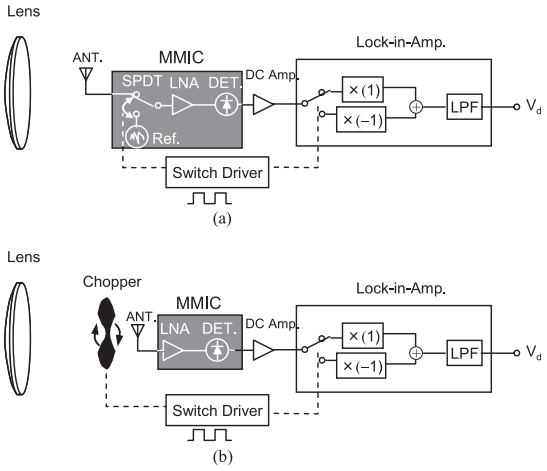

Fig. 12 (a) Block diagram of PMMW imager with electronic switch. (b) Block diagram of PMMW imager with mechanical chopper.

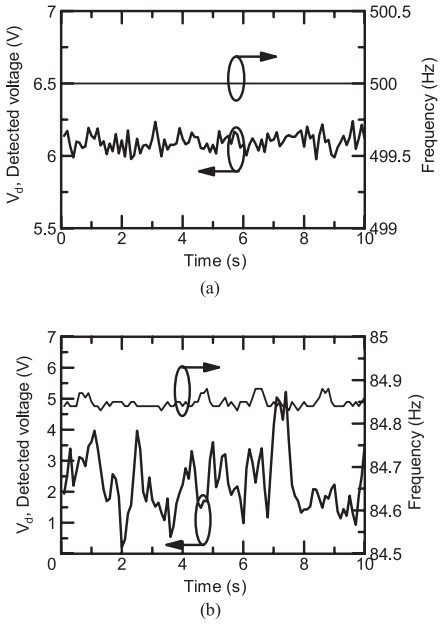

Fig. 13 Measured detected voltage and frequency from the lock-in amplifier: (a) using an electrical switch; (b) using a mechanical chopper.

the minimum detectable temperature difference (ΔT). This large variation was caused by variations in the rotational speed due to eccentricity or imbalances in the weight of the chopper. The detected frequency also has variations as shown in Fig. 13(b). In addition, the chopper also vibrates, which generates noise. On the other hands, the fluctuations in the voltage detected using the electrical switch are within 0.25 V_{pp} as shown in Fig 13(a). Thus, a small ΔT is possible using the PMMW imager with electronic switch.

We acquired millimeter-wave images of a person with a concealed metal object (simulating a gun) using an imager with an electronic switch in Fig. 14(a) and a mechanical chopper in Fig. 14(b). The distance between the target and the receiver was 2.5 m, the image size was 40 ×

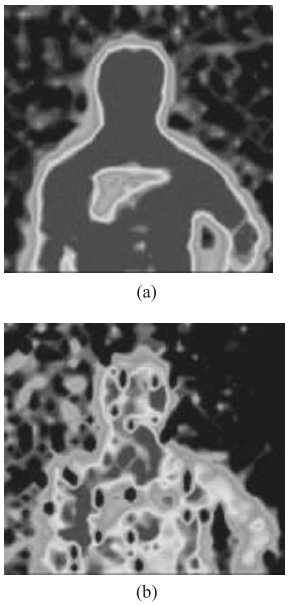

(a)

(b)

Fig. 14 PMMW images of a person with a concealed metal object. (a) Captured by the imager shown in Fig. 11(a). (b) Captured by the imager shown in Fig. 11 (b).

Table 1 Noise temperature of the system components.

	Noise temperature, K
Lens loss	33
Coupling loss	182
Transition loss	95.4
Insertion loss in switch	175
Noise temperature in LNA	298
Overall noise temperature	1936

40 pixels, and the spot size on the target was 2 cm. The blue areas represent colder radiometric temperatures for the sample metal object and the ambient temperature, and the red areas represent warmer temperatures. As you can see, the millimeter-wave image captured by the imager with the electronic switch shown in Fig. 14(a) has a much higher resolution than one captured by the imager with the mechanical chopper shown in Fig. 14(b).

The image collection times for the millimeter-wave images shown in Figs. 14(a) and (b) were 400 sec and 25 minutes, respectively. A PMMW imager with an MMIC receiver is able to achieve high-resolution millimeter-wave images in a much shorter image collection time. We also constructed a receiver array using 32 receivers, which reduced the image collection time within 10 sec.

Here is a summary of the system noise in our receiver. All the noise derived from the lens, the antenna including the coupling efficiency with the lens, the transition between the antenna and the MMIC, and the insertion loss in the switch increase the system noise. The noise temperature in each component is summarized in Table 1. From this table, the system NF was calculated as 8.7 dB.

4. Conclusions

We developed an MMIC receiver for a PMMW imaging system. To obtain high-resolution millimeter-wave images in a short image collection time, we developed an MMIC receiver with an electronic SPDT switch. The insertion loss and isolation of the switch were 2 dB and −40 dB, respectively, and the switching speed was more than 500 kHz. We also developed a high-gain low-noise amplifier using a 0.1 μm InP HEMT. The gain and noise figure measured at a frequency of 94 GHz were 35 dB and 3 dB, respectively. By integrating the SPDT switch with the LNA and detector, we developed a single-chip MMIC receiver.

Our configuration produced higher resolution millimeter-wave images in a much shorter integration time compared with the conventional configuration with the mechanical chopper.

Acknowledgments

The authors would like to thank all members of Fujitsu Laboratories' device-processing group for the fabrication. The authors would also like to thank Yutaka Toku for fabrication and measurements and Kazukiyo Joshin and Naoki Hara for their support. This work was supported by the Ministry of Internal Affairs and Communications under the Strategic Information and Communications R&D Promotion Programme (SCOPE).

References

[1] K. Mizuno, H. Matono, Y. Wagatsuma, H. Warashina, H. Sato, S. Miyanaga, and Y. Yamanaka, "New applications of millimeter-wave incoherent imaging," 2005 IEEE MTT-S Int. Microwave Symp. Digest, WE2C-3, June 2005.

[2] W.J. Wilson, R.J. Howard, A.C. Ibbott, G.S. Parks, and W.B. Ricketts, "Millimeter-wave imaging sensor," IEEE Trans. Microw. Theory Tech., vol.MTT-34, no.10, pp.1026–1035, 1986.

[3] D.R. Vizard and R. Doyle, "Advances in millimeter wave imaging and radar systems for civil applications," 2006 IEEE MTT-S Int. Microwave Symp. Digest, pp.94–97, June 2006.

[4] L. Yujiri, "Passive millimeter wave imaging," 2006 IEEE MTT-S Int. Microwave Symp. Digest, pp.98–101, June 2006.

[5] J.A. Lovberg, C. Martin, and V. Kolinko, "Vidio-rate passive millimeter-wave imaging using phased arrays," 2007 IEEE MTT-S Int. Microwave Symp. Digest, pp.1689–1692, June 2007.

[6] M. Sato, T. Hirose, T. Ohki, H. Sato, K. Sawaya, and K. Mizuno, "94-GHz band high-gain and low-noise amplifier using InP-HEMTs for passive millimeter wave imager," 2007 IEEE MTT-S Int. Microwave Symp. Digest, pp.1775–1778, June 2007.

[7] M. Sato, T. Hirose, T. Ohki, T. Takahashi, K. Makiyama, N. Hara, H. Sato, K. Sawaya, and K. Mizuno, "InP-HEMT MMICs for passive millimeter-wave imaging sensors," 2008 International Conference on Indium Phosphide and Related Materials, May 2008.

[8] M.E. Tiuri, "Radio astronomy receivers," IEEE Trans. Antennas Propag., vol.12, no.7, pp.930–938, Dec. 1964.

[9] H. Mizutani and Y. Takayama, "DC-110-GHz MMIC traveling-wave switch," IEEE Trans. Microw. Theory Tech., vol.48, no.5, pp.840–845, May 2000.

[10] S. Chang, J. Chen, H. Kuo, and H. Hsu, "A filter synthesis method applied to millimeter-wave Distributed switch design," 33rd European Microwave Conference, pp.1295–1298, Oct. 2003.
[11] H. Mizutani, N. Iwata, Y. Takayama, and K. Honjo, "Design considerations for traveling-wave single-pole multithrow MMIC switch using fully distributed FET," IEEE Trans. Microw. Theory Tech., vol.55, no.4, pp.664–671, April 2007.
[12] T. Takahashi, K. Makiyama, N. Hara, M. Sato, and T. Hirose, "Improvement in high frequency and noise characteristics of InP-based HEMTs by reducing parasitic capacitance," 2008 International Conference on Indium Phosphide and Related Materials, May 2008.
[13] Y. Itoh, K. Nakahara, T. Sakura, N. Yoshida, T. Katoh, T. Takagi, and Y. Ito, "W-band monolithic low noise amplifiers for advanced microwave scanning radiometer," IEEE Microw. Guid. Wave Lett., vol.5, no.2, pp.59–61, Feb. 1995.
[14] A. Tessmann, A. Leuther, C. Schwoerer, H. Massler, S. Kudszus, W. Reinert, and M. Schlechtweg, "A coplanar 94 GHz low-noise amplifier MMIC using 0.07 μm metamorphic cascode HEMTs," 2003 IEEE MTT-S Int. Microwave Symp. Dig., pp.1581–1584, June 2003.
[15] X.B. Mei, C.H. Lin, L.J. Lee, Y.M. Kim, P.H. Liu, M. Lange, A. Cavus, R. To, M. Nishimoto, and R. Lai, "A W-band InGaAs/InAlAs/InP HEMT low-noise amplifier MMIC with 2.5 dB noise figure and 19.4 dB gain at 94 GHz," 2008 Internal Conference on Indium Phosphide and Related Materials, May 2008.
[16] A. Tessmann, M. Kuri, M. Riessle, H. Massler, M. Zink, W. Reinert, W. Bronner, and A. Leuther, "A compact W-band dual-channel receiver module," 2006 IEEE MTT-S Int. Microwave Symp. Dig., pp.85–88, June 2006.
[17] M. Biedenbender, R. Lai, J. Lee, S. Chen, K.L. Tan, P.H. Liu, A. Freudenthal, D.C. Streit, B. Allen, and H. Wang, "A 0.1 μm W-band HEMT production process for high yield and high performance low noise and power MMICs,"1994 IEEE GaAs IC Symposium, Digest, pp.325–328, 1994.
[18] D.-W. Tu, W.P. Berk, S.E. Brown, N.E. Byer, S.W. Duncan, A. Eskandarian, E. Fischer, D.M. Gill, B. Golja, B.C. Kane, S.P. Svensson, and Weinreb, "High gain monolithic P-HEMT W-Band four-stage low noise amplifiers," 1994 IEEE Microwave and Millimeter-Wave Monolithic Circuits Symposium, Digest, pp.29–32, May 1994.
[19] D.C.W. Lo, G.S. Dow, B.R. Allen, L. Yujiri, M. Mussetto, T.W. Huang, H. Wang, and M. Biedenbender, "A monolithic W-band high-gain LNA/detector for millimeter wave radiometric imaging applications," 1995 IEEE MTT-S Int. Microwave Symp. Dig., pp.1117–1120, June 1995.

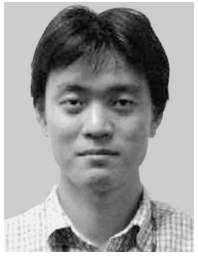

Masaru Sato received the B.E. and M.E. degrees in electrical engineering from Tohoku University, Sendai, Japan, in 1996 and 1999, respectively. He joined Fujitsu Laboratories Ltd., Atsugi, Japan in 1999 and has been engaged in research on high-speed InP-based HEMT circuits for fiber-optic communication systems and millimeter-wave integrated circuits. His current research interests include development of microwave and millimeter wave MMICs. He received the Young Researcher's Award from the IEICE in 2006.

Tatsuya Hirose received the B.E. degree from Tokyo Denki University, Tokyo, Japan, in 1987, and the M.E. degree from Hokkaido University, Sapporo, Japan, in 1989. He received the Ph.D. degree in electrical engineering from Tohoku University, Sendai, Japan, in 2004. In 1989, he joined Fujitsu Laboratories, Ltd., Kanagawa, Japan, where he has been engaged in research on the design and modeling of HEMTs and the development of MMICs based on their technologies. His current research interests include high-speed and high-frequency integrated circuits for optical and wireless communication systems. He is a member of the IEEE. Dr. Hirose received the 2003 Outstanding Young Engineer's Award from MTT-S.

Koji Mizuno received the B.E., M.E., and D.E. degrees in electronic engineering from Tohoku University, Sendai, Japan, in 1963, 1965, and 1968, respectively. In 1968, he joined the Department of Electronic Engineering, Faculty of Engineering, Tohoku University. In 1972, he became an Associate Professor with the Research Institute of Electrical Communication, Tohoku University where, since 1984, he was Professor of electron devices. In 1973, he spent a one-year sabbatical leave with Queen Mary College, University of London, under the sponsorship of Science Research Council (SRC, U.K.). In 1990, he spent a six-month sabbatical leave with the California Institute of Technology, Pasadena, and Queen Mary and Westfield College, London, under the sponsorship of Monbusho (Ministry of Education, Science, and Culture, Japan). From 1990 to 1998, he was a Team Leader of the Photodynamics Research Center, Institute of Physical and Chemical Research (RIKEN), Sendai, Japan, during which time he ran a laboratory for sub-millimeter-wave research there, as well as a laboratory with Tohoku University. He is now Professor emeritus and Research Professor of Tohoku University. His research interests concern the millimeter and sub-millimeter wave region of the electromagnetic wave spectrum, and he is currently involved in detection, generation, and applications in the region. Dr. Mizuno is a member of the Institute of Electrical Engineers of Japan, and the Japan Society of Applied Physics. He was the recipient of the Kenneth J. Button Medal in 1998, the Minister Award of MEXT (Ministry of Education, Culture, Science and Technology, Japan) in 2003, and the IEEE MTT-Society Distinguished Educator Award in 2005.